

# CnaA domains in bacterial pili are efficient dissipaters of large mechanical shocks

Daniel J. Echelman<sup>a,1,2</sup>, Jorge Alegre-Cebollada<sup>a,b,1,2</sup>, Carmen L. Badilla<sup>a</sup>, Chungyu Chang<sup>c</sup>, Hung Ton-That<sup>c</sup>, and Julio M. Fernández<sup>a,2</sup>

<sup>a</sup>Department of Biological Sciences, Columbia University, New York, NY 10027; <sup>b</sup>Centro Nacional de Investigaciones Cardiovasculares Carlos III (CNIC), 28029 Madrid, Spain; and <sup>c</sup>Department of Microbiology and Molecular Genetics, University of Texas–Houston Medical School, Houston, TX 77030

Edited by Scott J. Hultgren, Washington University School of Medicine, St. Louis, MO, and approved January 15, 2016 (received for review November 28, 2015)

**Pathogenic bacteria adhere despite severe mechanical perturbations induced by the host, such as coughing. In Gram-positive bacteria, extracellular protein appendages termed pili are necessary for adherence under mechanical stress. However, little is known about the behavior of Gram-positive pili under force. Here, we demonstrate a mechanism by which Gram-positive pili are able to dissipate mechanical energy through mechanical unfolding and refolding of isopeptide bond-delimited polypeptide loops present in Ig-type CnaA domains. Using single-molecule force spectroscopy, we find that these loops of the pilus subunit SpaA of the SpaA-type pilus from *Corynebacterium diphtheriae* and FimA of the type 2 pilus from *Actinomyces oris* unfold and extend at forces that are the highest yet reported for globular proteins. Loop refolding is limited by the hydrophobic collapse of the polypeptide and occurs in milliseconds. Remarkably, both SpaA and FimA initially refold to mechanically weaker intermediates that recover strength with time or ligand binding. Based on the high force extensibility, CnaA-containing pili can dissipate ~28-fold as much energy compared with their inextensible counterparts before reaching forces sufficient to cleave covalent bonds. We propose that efficient mechanical energy dissipation is key for sustained bacterial attachment against mechanical perturbations.**

bacterial adhesion | mechanical stability | single-molecule force spectroscopy | Gram-positive pili | isopeptide bond

**B**acterial infections of solid tissues begin with the attachment of bacteria to target surfaces. In many instances, bacteria adhere against forces that oppose such attachment: micturition in the genitourinary tract (1) or mucociliary flow in the respiratory tract (2), for example. In such environments, a completely immobile adherent bacterium experiences a drag force that can be approximated by Stokes law,  $F = 6\pi r\eta v$ , where  $r$  is the Stokes radius of the bacterium (~0.5  $\mu\text{m}$ ),  $\eta$  is the viscosity of the fluid (in the respiratory mucus, 1–100  $\text{Pa}\cdot\text{s}^{-1}$ ) (3), and  $v$  is the velocity of the fluid surrounding the bacterium (Fig. 1A). Under normal mucociliary flow (1–100  $\mu\text{m}\cdot\text{s}^{-1}$ ) (4), forces on a single bacterium can exceed several nanonewtons. Such high forces are sufficient to cleave covalent bonds within the initial adherence structures (5), which would terminate attachment. Understanding how bacteria manage to remain attached under such strong mechanical perturbations is of fundamental interest and could identify new targets for antibiotic development.

The initial interaction between bacteria and the host is mediated by micrometer-long adhesive structures termed pili or fimbriae (Fig. 1A). Due to their adhesive role, pili are virulence factors that contribute to the development of infections (6). Structurally, pili are polymers of tens to hundreds of subunits, termed shaft pilins, that are assembled in series and are presented at the extracellular surface, often with inclusion of minor pilins that can have adhesive properties (6). Remarkably, *Streptococcus agalactiae* strains that express adhesive pilins but lack shaft pilins show reduced attachment to respiratory epithelial cells, but only under flow conditions imitating in vivo mucus clearance (7). These findings suggest that shaft pilins, although not directly involved in the adhesion–ligand interaction, are nevertheless indispensable to the survival of the adhesive junction under mechanical stress. Indeed, these

shaft pilins are an emerging target for new vaccine and anti-adhesive development (8, 9).

In Gram-positive bacteria, pili polymerize via intermolecular isopeptide bonds. These covalent bonds link the  $\epsilon$ -amino group of a conserved Lys in one pilin with the peptide backbone of a conserved C-terminal Thr in a second pilin, and terminally form the covalent attachment to the bacterial cell wall (10). The result is a continuous covalent backbone and a circuit for mechanical forces to transmit axially from the distal ligand adhesion to the cell wall (11, 12) (Fig. 1B). Notably, as polymers of isopeptide bond-linked subunits, Gram-positive pili can reach sizes of the largest known polypeptides. For example, the type 2 pilus of *Actinomyces oris* can grow to lengths in excess of 2  $\mu\text{m}$  (13), thereby comprising an estimated >250 pilins along its axis and measuring >12 MDa.

Distinct from their Gram-positive counterparts, the pili of Gram-negative bacteria polymerize via strand–swap interactions and have a helical quaternary structure that unwinds under force to reduce strain on the bonds and prolong the adhesive junction (6, 14, 15). However, because the linear fiber-like pili of Gram-positive bacteria lack quaternary-level organization (16), it remains largely unknown how these megadalton-scale structures address the mechanical challenges for sustained adhesion.

Structures of 11 Gram-positive shaft pilins have been solved, revealing high structural similarity despite low sequence homology (17). All shaft pilins are multidomain proteins containing at least one CnaB Ig-type domain. Force-bearing CnaB domains harbor intramolecular Lys–Asp/Asn isopeptide bonds (18). Using the shaft pilin Spy0128 of *Streptococcus pyogenes*, we determined that CnaB domains are mechanically inextensible due to the location of the intramolecular isopeptide bonds, which bridge the

## Significance

**Bacteria colonizing the oropharynx must adhere despite mechanical challenges from coughing, sneezing, and chewing; however, little is known about how Gram-positive organisms achieve this feat. We studied the pilus adhesive proteins from two Gram-positive organisms and report a conserved mechanism for dissipating the energy of a mechanical perturbation. The two proteins are stable up to forces of 525 pN and 690 pN, respectively, making these proteins the most mechanically stable proteins known. After a perturbation, the proteins refold rapidly at low force, resulting in a large hysteresis with most of the unfolding energy lost as heat. The work presents an initial model whereby transient unfolding at forces of 500–700 pN dissipates mechanical energy and protects covalent bonds from cleavage.**

Author contributions: D.J.E., J.A.-C., and J.M.F. designed research; D.J.E., J.A.-C., and C.L.B. performed research; C.L.B., C.C., and H.T.-T. contributed new reagents/analytic tools; D.J.E., J.A.-C., and J.M.F. analyzed data; and D.J.E., J.A.-C., and J.M.F. wrote the paper.

The authors declare no conflict of interest.

This article is a PNAS Direct Submission.

<sup>1</sup>D.J.E. and J.A.-C. contributed equally to this work.

<sup>2</sup>To whom correspondence may be addressed. Email: dje2122@columbia.edu, jorge.alegre@cnic.es, or jfernandez@columbia.edu.

This article contains supporting information online at [www.pnas.org/lookup/suppl/doi:10.1073/pnas.1522946113/-DCSupplemental](http://www.pnas.org/lookup/suppl/doi:10.1073/pnas.1522946113/-DCSupplemental).

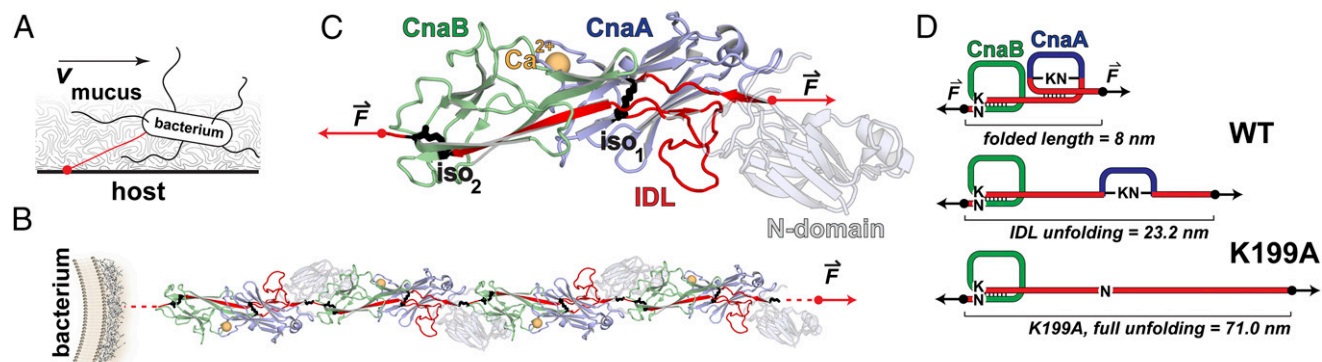


**Fig. 1.** Bacterial adhesion under mechanical force and the covalent architecture in pili of Gram-positive bacteria. (A) Schematic representation of a bacterium adhering to a host via a single pilus attachment. During a perturbation, such as coughing, the mucosal flow will be accelerated and will exert a drag force on the bacterium proportional to the velocity of the flow. This drag force propagates axially through the tethering pilus. (B) The SpaA-type pilus of *C. diphtheriae* is composed of multiple covalently linked SpaA pilins in series. The portion of each pilin that is subject to axial mechanical pulling begins only at Lys190, the site of the interpilin cross-link, and therefore does not involve the N-terminal domain. Ancillary pilins at the tip and at the base are not shown. (C) Structure of the SpaA pilin of *C. diphtheriae*. An intermolecular isopeptide bond between successive pilins is formed at Lys190 between the N-terminal domain and the CnaA, thereby removing the N-terminal domain from the pulling axis. Axial force propagates from Lys190 to the C terminus along the pathway shown in red, which includes an IDL in the CnaA domain, as well as intramolecular isopeptide bonds (black). A coordinated metal ion is shown as a yellow sphere [Protein Data Bank (PDB) ID code 3hr6]. (D) The folded SpaA pilin measures 8.0 nm from the interpilin cross-link to its C terminus. Of the 294 residues, 53 are unprotected by the Lys/Asn isopeptide bonds and can extend under mechanical force to a predicted 23.2 nm. The additional 122 residues of the CnaA domain can only extend in the absence of the K199/N321 isopeptide bond (K199A mutant), increasing the predicted extension to 71.0 nm.

N- and C-terminal  $\beta$ -strands (11). Therefore, a pilus containing only CnaB domains, such as in *S. pyogenes*, is predicted to be essentially inextensible.

However, 10 of 11 Gram-positive shaft pilins contain an additional CnaA Ig-type domain, with unknown consequences for the overall mechanical properties of the pilus (Fig. S1). CnaA domains also contain intramolecular isopeptide bonds. Unlike in CnaB domains, the intramolecular isopeptide of the CnaA domain bridges the first  $\beta$ -strand with the penultimate antiparallel  $\beta$ -strand. This arrangement generates a polypeptide loop that appears to lie in an axial force conduction pathway (Fig. 1C, red ribbon). We hypothesized that this “isopeptide-delimited loop” (IDL) of CnaA domains can be unfolded by mechanical force, giving extensibility to the Gram-positive pilus. Herein, we chose to investigate two CnaA-containing pilins, SpaA of *Corynebacterium diphtheriae* (diphtheria) and FimA of *Actinomyces oris* (dental plaque), because both originate from organisms that colonize the oropharynx, and thereby might be adapted to the large mechanical perturbations from coughing or chewing. Using single-molecule force spectroscopy by atomic force microscopy (AFM), we report that both pilins are mechanically extensible due to the unfolding of IDLs within their CnaA domains. Mechanical unfolding occurs at forces that are the highest reported so far for globular proteins. We also observe rapid refolding of the IDL into a mechanically distinct state. Given these unprecedented mechanical properties, we propose that CnaA domains are highly efficient shock absorbers for dissipating mechanical energy during mechanical perturbations, allowing adhesive junctions to persist against mechanical forces.

## Results

**SpaA-Type Pilus Has an Isopeptide-Delimited Extension at High Forces.** Internal isopeptide bonds are ubiquitous in the pili of Gram-positive bacteria. To date, mechanical study of these proteins has been limited to the Spy0128 shaft pilin of *S. pyogenes*, which is locked by two isopeptide bonds and has no extensible segment (11). However, most structures of Gram-positive shaft pilins reveal a polypeptide loop that is bounded between two isopeptide bonds (Fig. 1C), with unknown consequences for pilus mechanics.

We predicted that these IDLs could extend a limited amount based on an estimation of the extended length of the molecule minus the folded contour length. For example, the folded SpaA pilin from *C. diphtheriae* measures 8.0 nm from the C terminus in the crystal structure, at Lys484, to the interpilin cross-link, at

Lys190, where force propagates to the next subunit in the pilus (19) (Fig. 1D). Fully extended, the 294 residues from Lys190 to Lys484 would yield a predicted contour length of 117.6 nm, given 0.4 nm per amino acid (20). However, two isopeptide bonds would protect those residues sequestered behind them, a Lys199–Asn321 isopeptide bond protecting 122 residues and a Lys363–Asn482 isopeptide bond protecting another 119 residues. Consequently, of the 294 residues between Lys190 and Lys484, only 53 are unprotected by isopeptide bonds, which are mostly located to the IDL (Fig. 1C, red ribbon), and for which we would predict an extended contour length of 21.2 nm. Additional consideration for the length of the two isopeptide bonds, which measure up to 1.0 nm between the Lys and Asn  $\alpha$ -carbons in crystal structures (Fig. S2 and Table S1), increases the predicted extension to 23.2 nm. This predicted extension minus the initial folded length of 8 nm gives a predicted contour length increment on unfolding of 15.2 nm.

As the most direct test of this hypothesized extension, we applied single-molecule force spectroscopy to the native SpaA-type pili of *C. diphtheriae*. We purified pili from a strain of *C. diphtheriae* that could polymerize pili but not anchor them to the cell wall, instead shedding their pilus into the culture supernatant. These pili measure several microns in length, as imaged by EM, and thereby contain hundreds of SpaA pilins in series. The purified SpaA-type pili were adsorbed onto gold surfaces and stretched with AFM in force-extension mode, yielding sawtooth patterns composed of multiple force peaks spaced by equal length increments (Fig. 2A). The maximum force of each peak and the increment in contour length between peaks was recorded in every trace with such sawtooth-like patterns. A plot of the maximum force vs. contour length increment reveals a predominant population having  $14.0 \pm 0.8$ -nm unfoldings at a force of  $530 \pm 109$  pN (Fig. 2B and Fig. S3A and B).

If SpaA unfolding is isopeptide-delimited, removal of the isopeptide bond would increase the unfolded length by a predictable amount (e.g.,  $\sim 49$  nm due to the 122 amino acids released between the CnaA isopeptide residues, Lys199–Asn321). We therefore engineered and purified pili where the CnaA isopeptide-forming Lys was mutated out (SpaA K199A). With 175 residues and only one isopeptide now exposed to force, we predicted a full extension of 71.0 nm and a contour length increment on unfolding of 63.0 nm (Fig. 1D). In force extension, a single population of unfolding events emerges with  $60.6 \pm 0.4$ -nm contour length increments, and with a notably lower force of  $299 \pm 21$  pN (Fig. 2B and Fig. S3C and D). This observation of mechanical

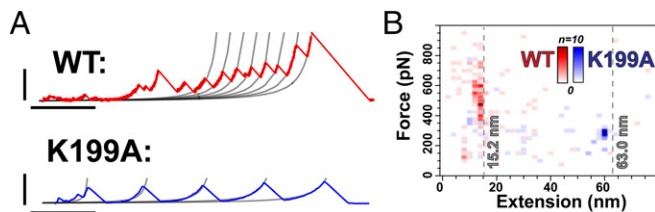


**Fig. 2.** SpaA-type pilus is fractionally extensible. (A) Force-extension traces of the purified WT SpaA pili and the SpaA K199A mutant pili. The black traces show fits to the worm-like chain model with 13.5-nm (WT) or 60-nm (K199A) contour length increments. (Vertical scale bars, 500 pN; horizontal scale bars, 60 nm.) (B) Bivariate histogram of the peak unfolding force vs. contour length increment for WT SpaA pili (red,  $n = 181$  unfolding peaks) and SpaA K199A pili (blue,  $n = 74$  unfolding peaks). The predicted contour length increments, the extended length minus the folded length, are indicated with dashed lines. Scale bars show the number of individual unfolding events.

weakening is consistent with molecular dynamics simulations that predict a decrease in the mechanical stability of the CnaB type domains of a *S. pyogenes* pilin upon loss of isopeptide bonds (21).

**IDL Unfolding Occurs at Unprecedented Forces.** There are several limitations inherent to the mechanical study of purified pili. Pili do not exclusively contain the SpaA shaft proteins, and measurements may be confounded by incorporated adhesins and other ancillary proteins (13). Moreover, the attachment of pili to the surface and cantilever relies on nonspecific interactions, such that the vector of the force is not explicitly defined. To overcome these limitations, we produced an engineered heteropolyprotein of the SpaA pilin with a C-terminal Cys for covalent attachment to gold-coated cantilevers, along with an N-terminal HaloTag protein that allows covalent tethering to functionalized glass surfaces (22, 23) (Fig. 3A). Such covalent anchorage ensures single-molecule tethers that can withstand forces close to 1 nN (23). Importantly, SpaA is pulled with the same geometry in the heteropolyprotein as in native pili.

Initial attempts to make a synthetic pilus-like HaloTag-(SpaA)<sub>4</sub>-Cys heteropolyprotein were complicated by poor protein expression. In turn, we flanked SpaA pilins with three I27 modules, which serve to enhance expression and also to provide an additional mechanical fingerprint (11) (Fig. 3A and B). In force extension, we observed a distinct population of sawtooth peaks with  $13.6 \pm 0.4$ -nm contour length increments at a force of  $525 \pm 65$  pN (Fig. 3C and Fig. S44). These results with the engineered SpaA heteropolyprotein are consistent with the measurements on native SpaA-type pili and with our structure-based predictions, and confirm that unfolding in SpaA is limited to the 53 residues not protected behind isopeptide bonds.

Of note, an additional population with unfolding increments of  $51.4 \pm 1.2$  nm at a force of  $71 \pm 17$  pN was observed (Figs. S44 and S5), which is in agreement with the predicted extension upon unfolding of the SpaA N-terminal domain ( $138 \text{ residues} \times 0.4 \text{ nm-residue}^{-1} - 3.1 \text{ nm of initial extension} = 52.1 \text{ nm}$ ). This N-terminal domain is not subject to axial force in the native SpaA-type pilus, where force propagates from one SpaA subunit to the next via an intermolecular isopeptide bond with Lys190, which is located immediately distal to this domain (Fig. 1C). As such, the role of the N-terminal domain is likely tangential to the mechanical function of the pilus shaft.

To explore whether such mechanical features are a general feature of CnaA-type pilin domains, we expanded our study to the shaft FimA pilin of the type 2 pilus of *A. oris* (24). We synthesized a pilus-like FimA polyprotein construct of four FimA pilins in series, along with an N-terminal HaloTag and a C-terminal Cys for covalent tethering (23) (Fig. 3D). When extended at a constant velocity of  $400 \text{ nm-s}^{-1}$ , the FimA construct yields a sawtooth-like pattern in the force vs. extension trace, with four peaks of equal spacing (Fig. 3E). The FimA pilin unfolds at an extraordinarily high force of  $690 \pm 70$  pN, with a contour length increment of  $14.2 \pm 0.6$  nm (Fig. 3F and Fig. S4B). In the FimA

crystal structure, 51 residues are unprotected by the isopeptide bonds, and the N and C termini are separated by 6.9 nm, giving a predicted unfolding extension of 15.5 nm ( $51 \text{ residues} \times 0.4 \text{ nm-residue}^{-1} + 2 \text{ isopeptides} \times 1.0 \text{ nm-isopeptide}^{-1} - 6.9 \text{ nm}$ ).

Thus, in both the SpaA and FimA shaft pilins, unfolding extensions are limited to the fraction of residues not protected behind isopeptide bonds. In the SpaA structure, 42 of the 53 unprotected residues fall in the IDL, with the remainder located before or after the isopeptides at the termini. In the FimA structure, 44 of 51 unprotected residues fall in the IDL. Moreover, the unprotected segments at the termini are already in extended or close to extended conformations in the SpaA and FimA crystal structures. Thus, it is most likely that the unfolding extensions and high mechanical stabilities owe largely to the unfolding of the IDLs of SpaA and FimA.

**SpaA and FimA Refold to a Mechanically Weak Intermediate.** The addition of internal covalent bonds has been demonstrated to accelerate the rate of folding (20, 25). We therefore asked whether the IDL, in addition to its high mechanical stability, had rapid refolding kinetics.

To measure SpaA and FimA refolding, we applied denature-quench-probe protocols using AFM-based force spectroscopy in “force-clamp” mode (26, 27). On the denature pulse, a high force ( $\geq 350$  pN) is applied to unfold the polyprotein, with individual events observed as  $\sim 12.5$ -nm steps in the extension vs. time trace. Next, a quench pulse with the force set at 0 pN allows for domain refolding. Domains that refold during the quench pulse are detected by their subsequent unfolding during the probe pulse. In a representative recording of FimA refolding, four steps are observed in the initial unfolding pulse and three steps are observed in the subsequent probe pulse, indicating that three of four domains refolded during the interspaced 50-ms quench pulse (Fig. 4A). Similarly, in a representative recording of the SpaA polyprotein, both SpaA domains unfold on the denature pulse and again on the probe pulse, having refolded during the 200-ms quench pulse (Fig. 4C). Unfolding of the I27 modules can be observed as 25-nm steps, although the kinetics of I27 refolding are slower and take several seconds (20).

We summed 47 recordings of FimA unfolding at 500 pN on denature pulses or on probe pulses (Fig. 4B). Unfolding events occur more rapidly on the probe pulse than on the denature pulse, suggesting a decreased mechanical stability of the refolded

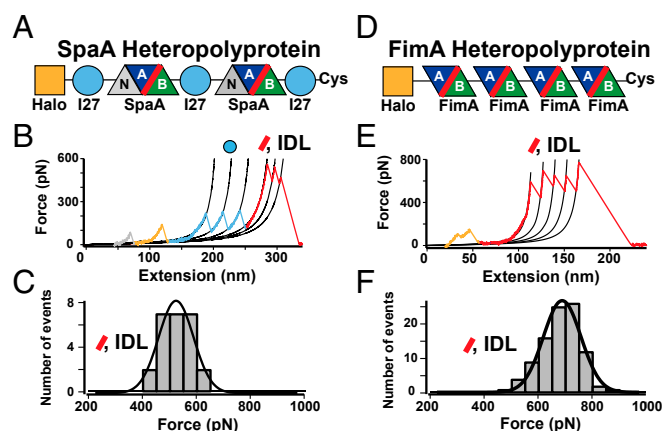
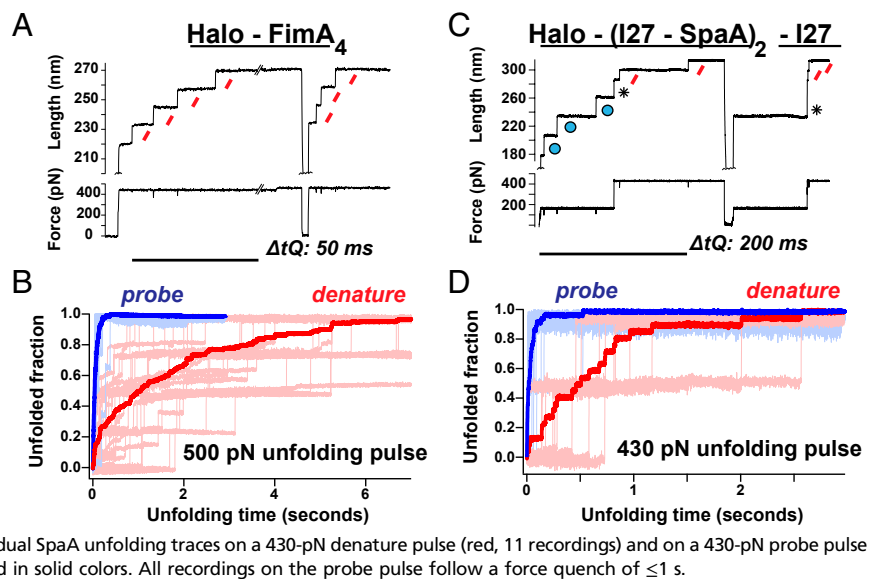


**Fig. 3.** Gram-positive pilins are extensible at unprecedented unfolding forces. Schematic representations of the SpaA polyprotein (A) and the FimA polyprotein (D), which include CnaA (A), CnaB (B), and N-terminal (N, SpaA only) domains. Red lines represent the IDL between the CnaA and CnaB domains (Fig. 1C). Force-extension recordings of the SpaA (B) and FimA (E) polyproteins with characteristic sawtooth unfolding patterns. Worm-like chain fits have 14-nm (red, IDL) or 29-nm (blue, I27) contour length increments. Histograms of the SpaA (C,  $n = 25$ ) and FimA (F,  $n = 96$ ) unfolding forces for the peaks that preceded the 14-nm contour length increments are shown. Black lines show Gaussian fits.

**Fig. 4.** FimA and SpaA refold to mechanically weaker intermediates. (A) Representative force-clamp recording of the FimA polyprotein showing a high-force unfolding pulse, followed by a 50-ms low-force refolding pulse ( $\Delta t_Q$ ) and a second high-force unfolding pulse. FimA IDL unfolding is identifiable as  $\sim 12.5$ -nm stepwise length increments (red slashes). (Scale bar, 1 s.) (B) Faded traces show individual FimA unfolding traces on a 500-pN denature pulse (red, 27 recordings) and on a 500-pN probe pulse (blue, 20 recordings), with the normalized sums depicted in solid colors. All recordings on the probe pulse follow a 1-s force quench. (C) Representative force-clamp recording of the SpaA polyprotein. Two forces are applied on both the denature and probe pulses, an initial low-force pulse (165 pN) to unfold the I27 domains and a later high-force pulse (430 pN) to unfold the SpaA pilins. I27 unfolding is identifiable as  $\sim 25$ -nm stepwise length increments (blue circle), and SpaA unfolding is identifiable as  $\sim 12.5$ -nm stepwise length increments (red slashes). (Scale bar, 4 s.) Steps identified with asterisks correspond to entropic increases in the length of the polyprotein due to the change in the applied force. (D) Faded traces show individual SpaA unfolding traces on a 430-pN denature pulse (red, 11 recordings) and on a 430-pN probe pulse (blue, 20 recordings), with the normalized sums depicted in solid colors. All recordings on the probe pulse follow a force quench of  $\leq 1$  s.



domains. To measure the respective unfolding rates, we summed all of the extension vs. time recordings and then fit this sum with a single exponential. FimA unfolds at a rate of  $0.58 \pm 0.12 \text{ s}^{-1}$  on the denature pulse at 500 pN, and at a rate of  $17.43 \pm 2.37 \text{ s}^{-1}$  on the probe pulse at 500 pN (Fig. 4B). A similar phenomenon was observed for SpaA, which unfolds at a rate of  $1.63 \pm 0.41 \text{ s}^{-1}$  on the denature pulse at 430 pN, and at a rate of  $30.38 \pm 7.98 \text{ s}^{-1}$  on the probe pulse at 430 pN (Fig. 4D). This discrepancy in unfolding rates between the denature pulse and the probe pulse indicates that both FimA and SpaA pilins exist in a weaker state immediately upon refolding.

We resolved the refolding kinetics of both pilins by varying the time of the quench pulse,  $\Delta t_Q$ , and counting the number of steps recovered on the probe pulse. Refolding of SpaA and FimA proceeds rapidly, approaching completion after 100 ms. However, refolding is only observed in proteins that collapse from their mechanically extended state (Fig. S6A). Only after a polypeptide collapses beyond  $\sim 60\%$  of its unfolded length does protein folding become appreciable (Fig. S6B and D). We have proposed before that mechanical folding of proteins is a two-step process, where actual folding is preceded by the hydrophobic collapse of the extended polypeptide (28, 29). We therefore considered the time course of refolding in only those traces that collapsed more than 60% of their unfolded lengths. Beyond that threshold, the FimA pilin refolds at a rate of at least  $17 \text{ s}^{-1}$ , whereas the SpaA pilin refolds at a rate of at least  $14 \text{ s}^{-1}$  (Fig. S6C and E). These rates are lower bound estimates of the actual folding rate, because our measurements are limited by the time it takes for the polypeptide to collapse. Even so, these refolding rates are one order of magnitude faster than other mechanical proteins studied using force spectroscopy, such as the titin I27 domain and ubiquitin (20, 29). Internal isopeptide bonds are likely critical to this rapid refolding; indeed, refolding accelerates when internal covalent bonds are engineered into proteins (20, 25).

**Maturation of CnaA Domains to the Native Fold Is Slow.** The native unfolding on the denature pulse and the weaker unfolding on the probe pulse are each observed as individual  $\sim 12.5$ -nm steps in force clamp. To differentiate between the two populations, we implemented refolding experiments using a linear increasing ramp in the force ( $100 \text{ pN}\cdot\text{s}^{-1}$ ), or “force ramp.” This technique allows us to discern the relative mechanical stability of domains in the denature and probe pulses by measuring the force at which they unfold on the ramp (27). In a representative recording of a force-ramp refolding experiment, a single FimA polyprotein is subject to three unfolding/refolding cycles alternating 1-s and 20-s

quench pulses (Fig. 5A). Four  $\sim 12.5$ -nm steps are observed on the denature pulse and on each subsequent probe pulse, indicating 100% refolding on the three quench pulses. In this trace, mechanical stability of FimA appears to depend on the duration of the quench pulse. All four events on the denature pulse are seen at  $>500$  pN, whereas all four events occur at  $<500$  pN after a 1-s quench pulse. With a 20-s quench pulse, two of four events unfold at forces above 500 pN, yet all return to the weak state after a subsequent 1-s quench pulse.

We aggregated the data from 135 recordings to explore the kinetics of maturation of the mechanical stability of FimA. FimA unfolding steps occur at  $563 \pm 46$  pN on the denature force ramp, which drops to  $438 \pm 38$  pN on the probe force ramp following a 1-s quench pulse (Fig. 5B). The fraction of events that occur at high force increases with the duration of the quench pulse (Fig. 5B). Considering these two populations of stabilities as two states of FimA, a native strong state that is present on the initial denature pulse and an intermediate weak state only present on the probe pulse, we modeled a first-order kinetic process for the maturation of the FimA intermediate state at a rate of  $0.011 \text{ s}^{-1}$  (Fig. S7B). Similarly, SpaA unfolding events occur at a higher force on a denature force ramp,  $453 \pm 46$  pN, than on a probe force ramp after a  $\Delta t_Q$  of 1 s,  $369 \pm 41$  pN (Fig. 5C). We also observed a time-dependent maturation of the mechanical stability of SpaA, although at a slower rate than FimA (Fig. S7A and B).

**Recovery of Mechanical Stability in SpaA Is Favored by  $\text{Ca}^{2+}$ .** Because coordinated metal cations are common among Gram-positive shaft pilins (Fig. S1), we examined whether metal binding is important for their mechanical properties. A coordinated metal ion is present in the SpaA crystal structure close to the interface between the CnaA and CnaB domains and just distal to Lys199 of the CnaA isopeptide bond (Fig. 1C). With a 2.48-Å metal-ligand bond distance, Kang et al. (19) postulated the presence of one  $\text{Ca}^{2+}$  ion, despite the lack of  $\text{Ca}^{2+}$  in the crystallization buffer. We hypothesized that mechanical unfolding may disrupt the  $\text{Ca}^{2+}$ -binding site of SpaA, releasing the metal ion into solution, where it would be sequestered by EDTA in the sample buffer. Hence, unfolding in the absence of calcium could yield an apo-form of SpaA with distinct mechanical properties. In contrast, refolding in the presence of  $\text{Ca}^{2+}$  would reconstitute the holo-form of SpaA. Supporting our hypothesis, we found that the mechanical stability decreases by  $\sim 20\%$  immediately after unfolding of SpaA. When the buffer is saturated with a 10-fold molar excess of calcium (10 mM) to EDTA (1 mM), refolded SpaA rapidly recovers a high mechanical stability state (Fig. 5C).

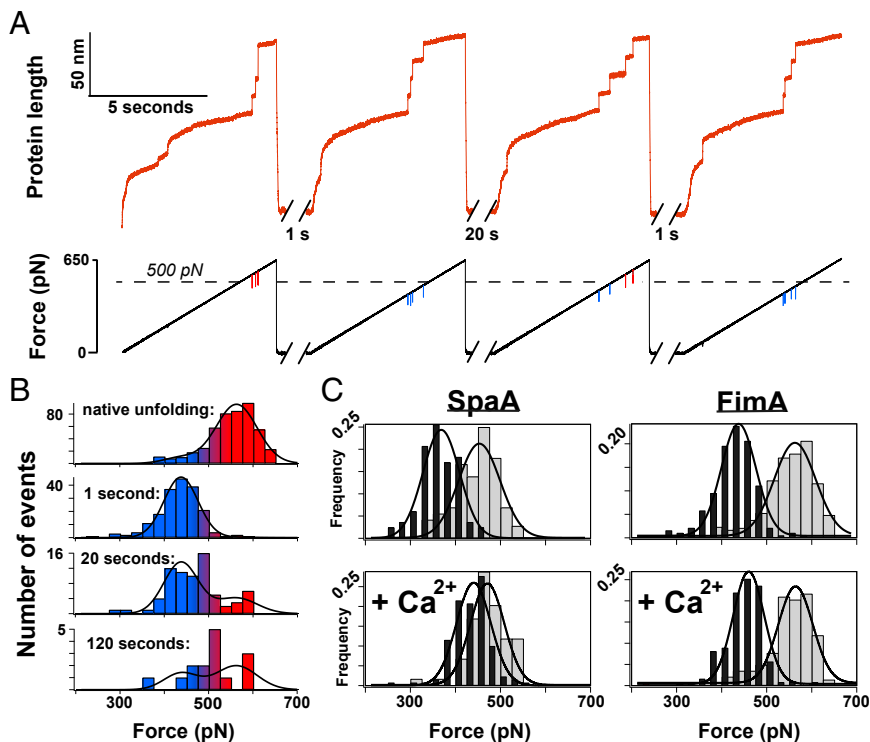


**Fig. 5.** Pilin recovery of native-like mechanical stability with time or ligand binding. (A) Representative trace showing unfolding force-ramp pulses separated by refolding pulses. (Bottom) Spikes in the force vs. time trace indicate the forces of IDL unfolding. Events above 500 pN are colored in red, and events below 500 pN are colored in blue. (B) Histograms of the force-ramp FimA unfolding forces on the first unfolding force pulse and after refolding pulses of variable durations. Events above 500 pN are colored in red, and events below 500 pN are colored in blue. The black lines represent fits to a double Gaussian function ( $n = 16$  at the 120-s time point,  $n \geq 70$  at other time points). (C) Histograms of the force-ramp unfolding forces on the initial denature ramp (gray) and on the probe ramp (black) following a 1-s quench pulse for both the SpaA and FimA pilins. Experiments were carried out in standard AFM buffer with 1 mM EDTA (Top) or were supplemented with 10 mM CaCl<sub>2</sub> (Bottom). Black lines indicate Gaussian fits to the data ( $n \geq 59$  in each histogram).

We conclude that mechanical unfolding of the IDL of SpaA triggers the release of the coordinated Ca<sup>2+</sup> ion. If refolding occurs in the absence of Ca<sup>2+</sup>, a mechanically weaker state of SpaA is acquired. In the case of FimA, which does not have a calcium-binding site, results of refolding experiments were not affected by the presence of calcium (Fig. 5C).

It remains to be determined whether the mechanically weak state serves a functional role in adherence. Binding of a calcium ion in SpaA accelerates recovery to the native state, and thereby circumvents this weak state. Coordinated calcium ions are present in five of 11 shaft pilin crystal structures (Fig. S1), suggesting a more general mechanism for this calcium-assisted folding.

## Discussion

When colonizing a host, the adhesive pili of bacteria endure intense mechanical pulses, such as those that originate from coughing for *C. diphtheriae* in the upper respiratory tract or from chewing for *A. oris* on the teeth. Gram-negative bacteria can withstand shearing force by uncoiling the helical quaternary structure of their pili, effectively lowering the stress on critical bonds (15). Because Gram-positive pili lack such quaternary structure, an alternate strategy for adherence under force is necessary. Here, we have demonstrated that shaft pilins containing CnaA domains are extensible at high forces through the mechanical unfolding of conserved IDLs. Ten of 11 solved structures of Gram-positive shaft pilins contain CnaA domains (Fig. S1), and it is likely IDL unfolding reflects a more general mechanism for Gram-positive bacterial adherence. How, then, do these IDL mechanics sustain adhesion against force transients?

IDL unfolding and extension provide a relative plateau in force during a mechanical perturbation. This plateau can be appreciated from the force vs. extension recordings. For example, force peaks for the FimA polypeptide are distributed around 690 pN until all four pilins have unfolded, after which the force rises until the tether breaks (Fig. 3E). The native FimA pili of *A. oris* measure 1–2  $\mu\text{m}$  in length, the equivalent of  $\sim 140$ –280 pilins polymerized in series, each  $\sim 7$  nm from the intermolecular cross-link to the C terminus (13). Without unfolding, such as in the CnaB Spy0128-type pilus of *S. pyogenes*, force extension

follows a worm-like chain contour that rises unimpeded into the nanonewton range, where the lifetimes of covalent bonds are brief (5). In the case of the SpaA or FimA pilus, successive unfolding of hundreds of CnaA domains plateaus this force at  $\sim 525$  pN or  $\sim 690$  pN, respectively, where covalent bond lifetimes are exponentially greater (Fig. 6).

With such high unfolding forces, the CnaA/CnaB pilins of Gram-positive bacteria constitute a class of ultramechanically stable proteins. To our knowledge, the 690-pN unfolding force of FimA at a pulling rate of  $400 \text{ nm}\cdot\text{s}^{-1}$  is the largest yet reported for a single globular protein. Previously, the highest mechanical

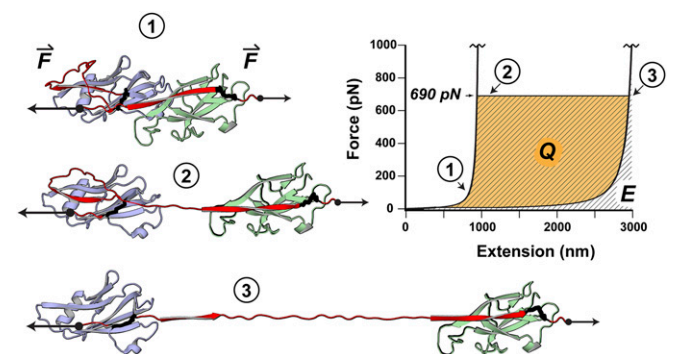


**Fig. 6.** CnaA unfolding provides a force plateau that prolongs the lifetime of the adhesive junction. In a 1- $\mu\text{m}$ -long FimA-type pilus, force on the folded FimA pilins (1) rises only up to  $\sim 690$  pN, at which point the extensible CnaA loops provide for an effective force plateau during their repeated unfolding (2). This secondary extension occurs away from equilibrium, with the additional work required to unfold the loops at high force being dissipated as heat (Q). After all CnaA loops have fully unfolded (3), the pilus may further extend up to a rupture force of  $\sim 1$  nN or may collapse along the worm-like chain contour of the extended polymer, with only a fraction of the total energy of the perturbation recovered as elastic energy (E). The unfolded structures (2 and 3) were rendered using molecular sculpting in PyMol based on the FimA crystal structure (PDB ID code 3qdh).

stabilities had been found in scaffoldin proteins of the microbial cellulosome. These proteins function in the cellular adhesion to crystalline cellulose substrates and are stable up to unfolding forces of 500 pN at equivalent pulling rates (30). In Gram-positive shaft pilins, such unprecedented unfolding forces would maximize the energy dissipated from a mechanical perturbation. Initial extension of a pilus occurs in equilibrium along the worm-like chain contour, with the work of extension transferred into elastic energy of the pilus. A mechanical perturbation of 0.05 fJ would extend a fully folded, 1- $\mu\text{m}$ -long pilus along this contour up to a force of 1 nN and covalent rupture (Fig. 6, 1). High-force unfolding of the 143 FimA domains in such a 1- $\mu\text{m}$ -long pilus would consume 1.38 fJ before reaching this 1-nN cutoff, an increase in efficiency of  $\sim 2,700\%$  (Fig. 6, 2). Only a fraction of the energy would be stored as elastic energy in the pilus, however. High force unfolding away from equilibrium yields a hysteresis with cyclic loading, with 1.23 fJ, or roughly 90%, dissipated as heat. After surviving a mechanical perturbation, CnaA domains collapse and rapidly refold, thereby priming the pilus for subsequent shocks.

Challenged with a mechanical perturbation of 1 fJ, the 1- $\mu\text{m}$ -long FimA pilus has a sufficient reserve of IDLs to dissipate the shock without overly stressing the covalent backbone. The energy needed to extend and unfold the pilus scales linearly with the length of the pilus shaft. A shorter FimA pilus would exhaust this reserve before spending the total energy of the perturbation. Therefore, from a mechanical point of view, pilus lengths may be tuned to a bacterium's environmental niche and the magnitude of the perturbations that it must withstand. Indeed, native pilus lengths vary widely. FimA pili are easily observed by EM in WT *A. oris*, and can exceed 2  $\mu\text{m}$  in length (13). Although other Gram-positive bacteria have shorter pili, the expression of genes responsible for pilus biogenesis may be up-regulated to produce longer pili (31, 32). One consequence of this observation is the hypothesis that pilus biogenesis is force-dependent, up-regulated only when longer pili are needed to dissipate large mechanical perturbations of the surrounding environment.

Ultimately, the remarkable mechanical properties of the pilus shaft must be complemented by a sufficiently strong adhesin–ligand interaction at the pilus tip. Recent structural and biochemical work has identified a conserved thioester bond in the adhesins from six Gram-positive genera, including *Corynebacterium* (33). These thioester bonds are present in putative binding pockets that are available to nucleophilic attack from amines, evoking the mechanism used by C3b and C4b complement proteins to anchor covalently to microbial surfaces (34). Two such streptococcal adhesins have been found to react with fibrinogen with high specificity to form intermolecular isopeptide bonds (33). This terminal intermolecular isopeptide at the tip of Gram-positive pili provides a continuous covalent backbone from the cell wall to the distal ligand attachment. The intense mechanical challenges induced by coughing or chewing would subject pili to nanonewton-scale forces sufficient to cleave covalent bonds and terminate the adhesive junction. As such, incorporation of CnaA-type domains along the pilus shaft therefore presents a unique mechanical strategy for withstanding these perturbations and dissipating the majority of their energy away as heat.

## Materials and Methods

Strains and primers used for native pilus expression are detailed in *SI Materials and Methods*. Pilus purification was based on a protocol described previously (35), and is further elaborated in *SI Materials and Methods*. SpaA and FimA polyproteins were engineered via multistep cloning involving BamHI, BglII, and KpnI restriction sites (29). Polyproteins were purified as described previously (23). Single-molecule AFM studies were conducted with a custom-built atomic force microscope (26) or on a commercially available atomic force microscope (Luigs and Neumann AG). Force-extension experiments were performed at a pulling speed of 400  $\text{nm}\cdot\text{s}^{-1}$ ; force-ramp experiments were performed at a loading rate of 100  $\text{pN}\cdot\text{s}^{-1}$ .

**ACKNOWLEDGMENTS.** This work was funded by NIH Grants HL66030, HL61228 (to J.M.F.), and AI106072 (to J.A.-C.); by National Institute of Dental and Craniofacial Research Grants DE017382 and DE025015 (to H.T.-T.); and by Marie Curie International Incoming Fellowship FP7-PEOPLE-2010-COFUND-267149 (to J.A.-C.).

- Thomas WE, Trintchina E, Forero M, Vogel V, Sokurenko EV (2002) Bacterial adhesion to target cells enhanced by shear force. *Cell* 109(7):913–923.
- Knowles MR, Boucher RC (2002) Mucus clearance as a primary innate defense mechanism for mammalian airways. *J Clin Invest* 109(5):571–577.
- Lai SK, Wang YY, Wirtz D, Hanes J (2009) Micro- and macrorheology of mucus. *Adv Drug Deliv Rev* 61(2):86–100.
- Cone RA (2009) Barrier properties of mucus. *Adv Drug Deliv Rev* 61(2):75–85.
- Grandbois M, Beyer M, Rief M, Clausen-Schaumann H, Gaub HE (1999) How strong is a covalent bond? *Science* 283(5408):1727–1730.
- Proft T, Baker EN (2009) Pili in Gram-negative and Gram-positive bacteria - structure, assembly and their role in disease. *Cell Mol Life Sci* 66(4):613–635.
- Konto-Ghiorgi Y, et al. (2009) Dual role for pilus in adherence to epithelial cells and biofilm formation in *Streptococcus agalactiae*. *PLoS Pathog* 5(5):e1000422.
- Nuccitelli A, et al. (2011) Structure-based approach to rationally design a chimeric protein for an effective vaccine against Group B *Streptococcus* infections. *Proc Natl Acad Sci USA* 108(25):10278–10283.
- Singh B, et al. (2015) Antibody-mediated disruption of the mechanics of CS20 fimbriae of enterotoxigenic *Escherichia coli*. *Sci Rep* 5:13678.
- Hendrickx APA, Budzik JM, Oh S-Y, Schneewind O (2011) Architects at the bacterial surface - sortases and the assembly of pili with isopeptide bonds. *Nat Rev Microbiol* 9(3):166–176.
- Alegre-Cebollada J, Badilla CL, Fernández JM (2010) Isopeptide bonds block the mechanical extension of pili in pathogenic *Streptococcus pyogenes*. *J Biol Chem* 285(15):11235–11242.
- Yeates TO, Clubb RT (2007) Biochemistry. How some pili pull. *Science* 318(5856):1558–1559.
- Reardon-Robinson ME, et al. (2014) Pilus hijacking by a bacterial coaggregation factor critical for oral biofilm development. *Proc Natl Acad Sci USA* 111(10):3835–3840.
- Whitfield MJ, Luo JP, Thomas WE (2014) Yielding elastic tethers stabilize robust cell adhesion. *PLoS Comput Biol* 10(12):e1003971.
- Zakrisson J, Wiklund K, Axner O, Andersson M (2012) Helix-like biopolymers can act as dampers of force for bacteria in flows. *Eur Biophys J* 41(6):551–560.
- Hilleringmann M, et al. (2009) Molecular architecture of *Streptococcus pneumoniae* TIGR4 pili. *EMBO J* 28(24):3921–3930.
- Cozzi R, et al. (2015) Structure and assembly of group B streptococcus pilus 2b backbone protein. *PLoS One* 10(5):e0125875.
- Kang HJ, Coulibaly F, Clow F, Proft T, Baker EN (2007) Stabilizing isopeptide bonds revealed in gram-positive bacterial pilus structure. *Science* 318(5856):1625–1628.
- Kang HJ, Paterson NG, Gaspar AH, Ton-That H, Baker EN (2009) The *Corynebacterium diphtheriae* shaft pilin SpaA is built of tandem Ig-like modules with stabilizing isopeptide and disulfide bonds. *Proc Natl Acad Sci USA* 106(40):16967–16971.
- Ainavarapu SR, et al. (2007) Contour length and refolding rate of a small protein controlled by engineered disulfide bonds. *Biophys J* 92(1):225–233.
- Wang B, Xiao S, Edwards SA, Gräter F (2013) Isopeptide bonds mechanically stabilize spy0128 in bacterial pili. *Biophys J* 104(9):2051–2057.
- Los GV, et al. (2008) HaloTag: A novel protein labeling technology for cell imaging and protein analysis. *ACS Chem Biol* 3(6):373–382.
- Popa I, et al. (2013) Nanomechanics of HaloTag tethers. *J Am Chem Soc* 135(34):12762–12771.
- Mishra A, et al. (2011) Two autonomous structural modules in the fimbrial shaft adhesin FimA mediate Actinomyces interactions with streptococci and host cells during oral biofilm development. *Mol Microbiol* 81(5):1205–1220.
- Kosuri P, et al. (2012) Protein folding drives disulfide formation. *Cell* 151(4):794–806.
- Popa I, Kosuri P, Alegre-Cebollada J, Garcia-Manyes S, Fernandez JM (2013) Force dependency of biochemical reactions measured by single-molecule force-clamp spectroscopy. *Nat Protoc* 8(7):1261–1276.
- Alegre-Cebollada J, et al. (2014) S-glutathionylation of cryptic cysteines enhances titin elasticity by blocking protein folding. *Cell* 156(6):1235–1246.
- Berkovich R, Garcia-Manyes S, Urbakh M, Klafter J, Fernandez JM (2010) Collapse dynamics of single proteins extended by force. *Biophys J* 98(11):2692–2701.
- Garcia-Manyes S, Dougan L, Badilla CL, Brujic J, Fernández JM (2009) Direct observation of an ensemble of stable collapsed states in the mechanical folding of ubiquitin. *Proc Natl Acad Sci USA* 106(26):10534–10539.
- Valbuena A, et al. (2009) On the remarkable mechanostability of scaffoldins and the mechanical clamp motif. *Proc Natl Acad Sci USA* 106(33):13791–13796.
- Gaspar AH, Ton-That H (2006) Assembly of distinct pilus structures on the surface of *Corynebacterium diphtheriae*. *J Bacteriol* 188(4):1526–1533.
- Ton-That H, Schneewind O (2003) Assembly of pili on the surface of *Corynebacterium diphtheriae*. *Mol Microbiol* 50(4):1429–1438.
- Walden M, et al. (2015) An internal thioester in a pathogen surface protein mediates covalent host binding. *eLife* 4:e06638.
- Linke-Winnebeck C, et al. (2014) Structural model for covalent adhesion of the *Streptococcus pyogenes* pilus through a thioester bond. *J Biol Chem* 289(1):177–189.
- Mandlik A, Das A, Ton-That H (2008) The molecular switch that activates the cell wall anchoring step of pilus assembly in gram-positive bacteria. *Proc Natl Acad Sci USA* 105(37):14147–14152.